



Article

Evaluation of Different ZX Tensile Coupon Designs in Additive Manufacturing of Amorphous and Semi-Crystalline Polymer Composites

Raviteja Rayaprolu ^{1,2}, Ajay Kumar Kadiyala ^{1,*} and Joseph G. Lawrence ^{1,3,*}

¹ Polymer Institute, The University of Toledo, Toledo, OH 43606, USA;
nagavenkatasairaviteja.rayaprolu@rockets.utoledo.edu

² Department of Mechanical, Industrial and Manufacturing Engineering, The University of Toledo,
Toledo, OH 43606, USA

³ Department of Chemical Engineering, The University of Toledo, Toledo, OH 43606, USA

* Correspondence: ajaykumar.kadiyala@utoledo.edu (A.K.K.); joseph.lawrence@utoledo.edu (J.G.L.)

Abstract: The layer-by-layer deposition of molten polymer filament in fused deposition modeling (FDM) has evolved as a disruptive technology for building complex parts. This technology has drawbacks such as the anisotropic property of the printed parts resulting in lower strength for parts printed in the vertical Z direction compared with the other two planes. In this manuscript, we attempt to address these challenges as well as the lack of standardization in sample preparation and mechanical testing of the printed parts. The paper focuses on process parameters and design optimization of the ZX build orientation. Type I tensile bars in ZX orientation were printed as per the ASTM D638 standard using two (2B) and four (4B) tensile bar designs. The proposed design reduces material loss and post-processing to extract the test coupons. Printing a type I tensile bar in the ZX orientation is more challenging than type IV and type V due to the increased length of the specimen and changes in additional heat buildup during layer-by-layer deposition. Three different polymer composite systems were studied: fast-crystallizing nanofiller-based high-temperature nylon (HTN), slow-crystallizing nanofiller-based polycyclohexylene diethylene terephthalate glycol-modified (PCTG), and amorphous carbon fiber-filled polyetherimide (PEI-CF). For all the polymer composite systems, the 2B showed the highest strength properties due to the shorter layer time aiding the diffusion in the interlayers. Further, rheological studies and SEM imaging were carried out to understand the influence of the two designs on fracture mechanics and interlayer bonding, providing valuable insights for the field of additive manufacturing and material science.

Keywords: FDM; FFF; ZX build orientation; type 1 tensile specimen; design optimization; layer time; print parameters; DOE



Citation: Rayaprolu, R.; Kadiyala, A.K.; Lawrence, J.G. Evaluation of Different ZX Tensile Coupon Designs in Additive Manufacturing of Amorphous and Semi-Crystalline Polymer Composites. *J. Compos. Sci.* **2024**, *8*, 379. <https://doi.org/10.3390/jcs8090379>

Academic Editor: Jeoung Han Kim

Received: 16 July 2024

Revised: 17 September 2024

Accepted: 20 September 2024

Published: 22 September 2024



Copyright: © 2024 by the authors. Licensee MDPI, Basel, Switzerland. This article is an open access article distributed under the terms and conditions of the Creative Commons Attribution (CC BY) license (<https://creativecommons.org/licenses/by/4.0/>).

1. Introduction

Material extrusion (MEX) manufacturing, also termed fused deposition modeling (FDM), is one of the seven additive manufacturing (AM) processes defined by ASTM. MEX is an additive manufacturing process in which material is dispensed through a nozzle or orifice, and the part is printed layer by layer. Material diversity, design customization freedom, higher production rates, and cost-effectiveness add advantages, allowing manufacturers to utilize FDM. Compared with traditional manufacturing methods, FDM is found useful for developing prototypes of functionally graded parts in different areas of research, including biomedical and dentistry, for building artificial bones [1], drug delivery studies [2], prosthetics, and temporary dental implant abutments [3,4].

The material properties, material handling, and control over the print process parameters are critical for obtaining good interlayer adhesion since FDM is a layer-by-layer deposition method. This results in parts with inferior, anisotropic properties compared

with conventional fabrication techniques. FDM processes can utilize both amorphous and semi-crystalline polymer, however, challenges remain with the necessity to have materials from engineering and high-performance thermoplastics to produce a fully functional part. This requires better print parameter optimization and understanding of part properties in the vertical Z orientation and better interlayer adhesion. The interlayer adhesion, in turn, significantly influences the inherent properties of the final part. Primary print process parameters like extrusion temperature, layer height, print speed, bed temperature, chamber temperature, and other advanced parameters including extrusion multiplier, road width, infill percentage, orientation [5,6], number of outlines [7], and other process settings directly affect the part strength and other properties. For an amorphous polymer, the diffusion process is governed by temperature. On the other hand, for a semi-crystalline polymer, both temperature and crystallization kinetics limit the diffusion process [8]. Crystallization is important for a semi-crystalline polymer since crystallinity improves the mechanical properties of the polymer [9]. In the case of engineering and high-performance amorphous polymers, it is important to maintain the chamber temperature at around the glass transition for better interlayer adhesion, as lower chamber temperatures can cool down the material below the glass transition, leading to poor interlayer adhesion. The same is true of semi-crystalline polymers, but crystallization rates govern the interlayer adhesion [10,11]. Further, semi-crystalline polymers exhibit higher shrinkage compared with the amorphous polymers due to the thermal gradient inherent in the printing process (rapid cooling), which can distort part stability and dimensional accuracy [12,13]. Hence, most semi-crystalline polymer feedstocks for FFF are altered to a pseudo-amorphous (behaves like an amorphous polymer) thermoplastic or filled with fillers. This has attracted research on high-performance polyether ketone (PEKK, pseudo-amorphous). However, there is very little literature available on polyether ether ketone (PEEK, semi-crystalline); polyphthalamide, a high-temperature nylon (HTN, semi-crystalline); and polyether imide (PEI, amorphous), which are suitable for engineering applications and those where the vertical build strength is critical. The research on PEI, HTN, PCTG, and their composites examines how process parameters [14–16], moisture content [17], and filler proportions [15,18] affect material properties, as well as the impact of these factors on samples produced in the ZX. There is a need to further understand the properties obtained and the stability of vertically built functional parts from these engineering polymers.

Traditional coupon testing methods are employed for AM parts to predict the printed part quality. However, these traditional methods fail to address AM parts' unique, unknown characteristics such as anisotropy in material property. The strength obtained in the ZX (vertical print direction) quantifies this layer-by-layer strength and is the weakest among other orientations (XY and YZ). Most researchers utilize an additional machining step to extract the dog-bone test coupon by printing a box. Data repeatability is a disadvantage of using the box method during property evaluation [19]. The tensile strength variation persists even after using the same process parameters and material handling methods. It can sometimes lead to conceptually incorrect conclusions [20]. Secondly, the box methods neglect optimizing retraction settings and do not provide an outlook on optimizing them, even though they play an essential role in printing complex geometries. The layer times also vary with the dimensions of the tower being printed, which can directly vary the properties of the tensile bars [21,22]. Finally, as the samples must be machined from the tower, the testing section is subjected to additional forces before tensile testing, which can produce incorrect and unreliable data. Material wastage and machining costs are other issues with this process. Hence, better standards are required to evaluate the tensile properties of FDM printed parts, or printing methods should be altered to build the test specimens [19].

A slight alternative to this method, proposed by Davies et al., is printing the type 1 tensile bars in the same tower format and machining the samples [19]. Although this method is considered a primary choice for printing tensile bars in the ZX build orientation, some necessary parameters are left unaddressed. Tensile bars with end tabs or dumbbell shapes tend to have increased stress concentrations in the curved sections, causing most

samples to fail at these points rather than the gauge section, which is the primary focus for tensile testing. Due to this consistent failure pattern, another standard, ASTM D3039, has been adopted for tensile testing. Unlike the D638 standard, ASTM D3039 employs a consistent rectangular geometry that more accurately determines material properties [23,24]. Numerous comparative studies between D638 and D3039 have been conducted using various polymers and composites. Miller et al. compared FDM samples printed with ABS using the ASTM D638 and D3039 standards to determine which is better suited for tensile testing of composites. The D3039 samples consistently met the failure acceptance criteria outlined in the standard across all builds. Conversely, the D638 samples exhibited increased randomness in break locations with longer test specimens, attributed to more potential crack nucleation sites [25]. In this paper, we try to address the gaps by developing customized design methodologies to overcome the challenges in printing the type 1 tensile bar in the ZX orientation. Two ZX designs were developed, the proposed design has minimal material wastage, and it requires no post-processing or machining to extract the test coupons. To validate the design, different polymer systems were considered: engineering and high-temperature thermoplastics polycyclohexylene diethylene terephthalate glycol-modified (PCTG), HTN, and carbon fiber-filled PEI. Initially, the influence of process parameters and optimization of process parameters was carried out. Further rheological studies were conducted to study the flow behavior and correlate the layer time analyses with tensile test results. SEM imaging was used to study the fracture surfaces after the tensile tests.

2. Materials and Methods

2.1. Materials

Three commercially obtained polymer composites, carbon fiber-filled PEI [PEI-CF], PCTG Z, and HTN Z (Z indicates the polymer's electrically conductive property), were selected to investigate the applicability of the designs proposed in Figure 1. Carbon fiber PEI represents amorphous thermoplastic, and PCTG Z and HTN Z represent semi-crystalline thermoplastic polymers (with differing crystallization kinetics). The PCTG Z and HTN Z are specialty nanocomposites/microcomposites blended with improved electrostatic dissipation properties. The exact composition of these specialty filaments is unknown due to the proprietary nature of the formulations.

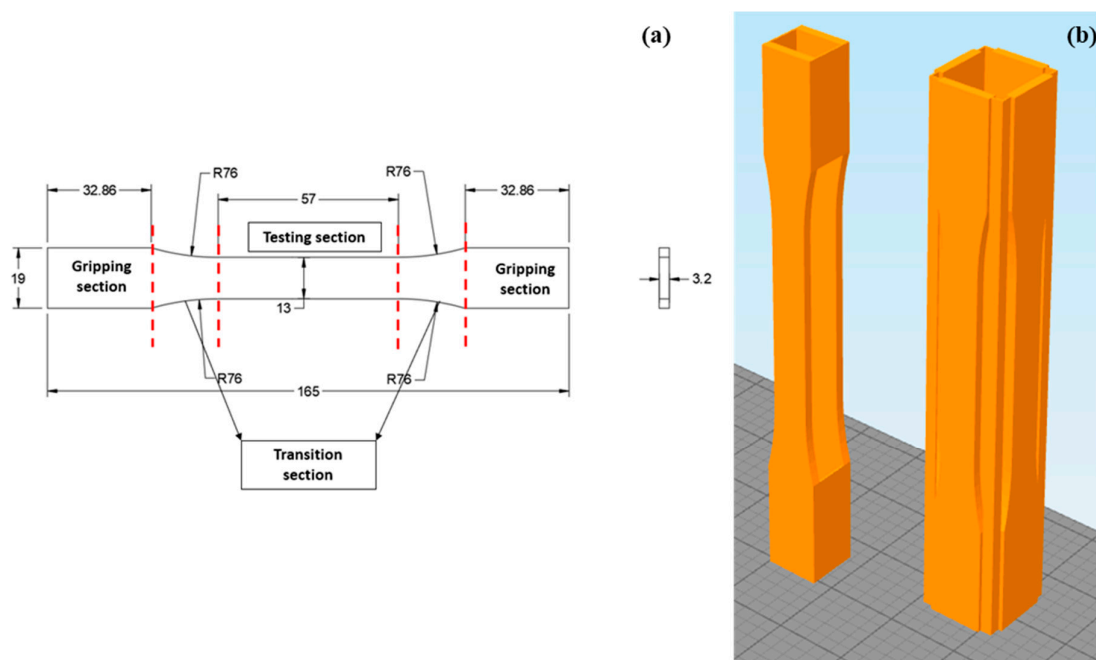


Figure 1. (a) Schematic of type 1 tensile bar dimensions; (b) two-bar (2B) and four-bar (4B) tensile bar designs for ZX orientation.

Amorphous thermoplastic PEI-CF was procured from 3DXTECH, USA. PCTG Z and HTN Z (high-temperature nylon) were procured from Essentium, USA.

2.2. Design Optimization

To address the challenges faced while printing a type 1 tensile bar in ZX orientation, two types of designs were considered, as shown in Figure 1b. Two-tensile-bar designs (2B) joined with two outline connections and a four-bar design (4B) with twelve were considered.

2.3. Process Parameters Optimization Using Design of Experiment (DoX)

All the samples in this study were printed using a Funmat HT enhanced 3D, USA printer. Prior to printing, all the filaments were vacuum dried overnight at their respective drying temperatures, as mentioned in the technical data sheet (TDS).

A mini-DoX (design of experiment) was conducted on the main process parameters used in the printing process. These include extrusion temperature, layer height, and print speed (Table 1). A two-factor, two-level, general factorial ANOVA DoX design that has four runs was constructed for all three materials considered, and the design was constructed to determine the optimum print process parameters for all three materials. Print speed was not considered as a factor and was kept constant at 40 mm/s for printing the DOE run order as per the design for all the composites. For each run order, a total of four samples were printed and tested.

Table 1. Process parameters of different composites considered for DOE.

Composite	Extrusion Temperature (°C)	Layer Height (mm)
PEI-CF	430, 450	0.2, 0.3
PCTG Z	290, 310	0.2, 0.3
HTN Z	320, 340	0.2, 0.3

2.4. Material Characterization and Testing

2.4.1. Rheology

The ARES-RDA from TA instruments was used for dynamic rheological property measurements using a 25 mm parallel plate. The plate gap was set at 2 mm, and the measurement temperatures for PCTC Z, HTN Z, and PEI-CF were 290 °C, 300 °C, and 380 °C, respectively. To determine the linear viscoelastic region (LVE), an oscillatory strain sweep was carried out. The oscillatory strain was varied from 0.01 to 100% at an angular frequency of 6.28 rad/s. A frequency sweep was carried out for all composites, and the frequency ranged from 0.1 to 500 rad/sec in the LVE region. Complex viscosity, storage modulus, and loss modulus were determined as a function of angular frequency. Steady state flow sweep was carried out from 0.1 to 500 s⁻¹ at the measurement temperatures mentioned above.

2.4.2. Scanning Electron Microscopy (SEM)

An FEI Quanta 3D FEG dual-beam microscope, USA was used to take the SEM images in high vacuum mode at 30 kV accelerating voltage. The samples were gold sputtered to avoid the effect of charge accumulation on the workpiece.

SEM was used to examine the fractured surface of the tensile-tested AM coupons at low magnifications of nearly 30× to compare the variation in interlayer adhesion and fracture mechanism for two- and four-tensile-bar designs printed using composites PCTG Z, HTN Z, and PEI-CF.

2.4.3. Mechanical Testing

The tensile tests were performed on the printed type 1 tensile bars using the Instron universal testing machine using a 50 kN capacity load cell as per the ASTM D638 standard with a strain rate of 5 mm/min.

3. Results

The nature of the polymer, flow properties, and constituent filler materials influences the printing of ZX samples. Among the polymer systems considered in this work, PCTG is a thermoplastic polyester elastomer that comes under the class of engineering polymer. It is characterized by its slow crystallization rate and can be printed as transparent parts. The crystallization rate can be increased under a controlled thermal annealing condition.

HTN is a class of high-temperature nylon that can be used at high operating temperatures for an extended period and is classified between engineering and high-performance polymers. They are mainly polyphthalamide (PPA)-based, semi-crystalline, aromatic polyamide. HTN is characterized by a fast crystallization rate with improved mechanical and thermal properties compared with standard nylons such as nylon 6 and nylon 6,6.

PEI is classified as a high-performance polymer that is amorphous in nature. PEI might require high chamber temperatures to achieve high-strength properties during 3D printing due to its high glass transition temperature.

Due to their different characteristics (semi crystalline, amorphous, fast, and slow rate of crystallization), these polymer systems were used in this study. The rheological data and mechanical test results are discussed based on the nature of the polymer.

3.1. Rheological Properties

Duty et al. [26] suggested the four basic requirements for printability of material: (i) The material must be extruded out of the nozzle. (ii) The extrudate should hold the predetermined shape. (iii) The extrudate must bridge a gap of specific length. (iv) The extrudate material should be geometrically stable during the cooling period. These criteria are mainly controlled by the flow properties/rheology of the polymer [27]. In the present study, dynamic shear sweep, dynamic frequency sweep, and steady state shear sweep were carried out. These studies provide sufficient information about the material printability, bead stability, and processing window, which are useful for optimization of the print parameters such as print speed and bed and chamber temperature.

In the dynamic rheological studies, the strain sweep characterizes the level of homogeneity in the polymer composites. For viscoelastic materials, the response is independent of strain up to a critical strain, beyond which a non-linear behavior is displayed. Figure 2a–c displays the PCTG Z, HTN Z, and PEI-CF responses during the strain sweep test. For PCTG Z (Figure 2a), both the storage (G') and loss modulus (G'') were of similar amplitude. With the increase in percentage strain, a decrease in both G' and G'' was observed, indicating structural breakdown of the polymer. At a higher percentage strain, G'' was found to be higher than G' , which indicates that the viscous component is more dominant beyond the critical strain. For HTN Z (Figure 2b), the elastic component (G') was dominant across the strain sweep. There is some fluctuation within the linear viscoelastic region for HTN Z due to the polyphthalamide-based blend composition of the commercial HTN Z filament used in this work. For PEI-CF (Figure 2c), G' and G'' showed marginal drops with an increase in percent strain around 10% strain, and the viscous component was more dominant than the elastic component across the strain sweep.

The flow of polymer during the material extrusion process is pressure-driven through a nozzle. For a Newtonian fluid, the wall shear rate is estimated by Equation (1).

$$\dot{\gamma}_w = \frac{4Q}{\pi r^3} \quad (1)$$

where, $\dot{\gamma}$ is shear rate, Q is the volumetric flow rate and r is the nozzle radius. The radius of the nozzle used in the present work was 0.3 mm. In general, the shear rate experienced in the nozzle is around 10^2 – 10^3 in a material extrusion process. Due to the shear thinning nature of the polymers, a Rabinowitsch correction is applied to the true shear rate for the power law model (Equation (2)), where n is the power index. For $n = 1$, the material

behavior is Newtonian; $n > 1$ represents shear thickening and $n < 1$ shear thinning. For printability, n should be less than 1, i.e., shear thinning.

$$\dot{\gamma}_\omega = \frac{3n+1}{4n} \frac{4Q}{\pi r^3} \quad (2)$$

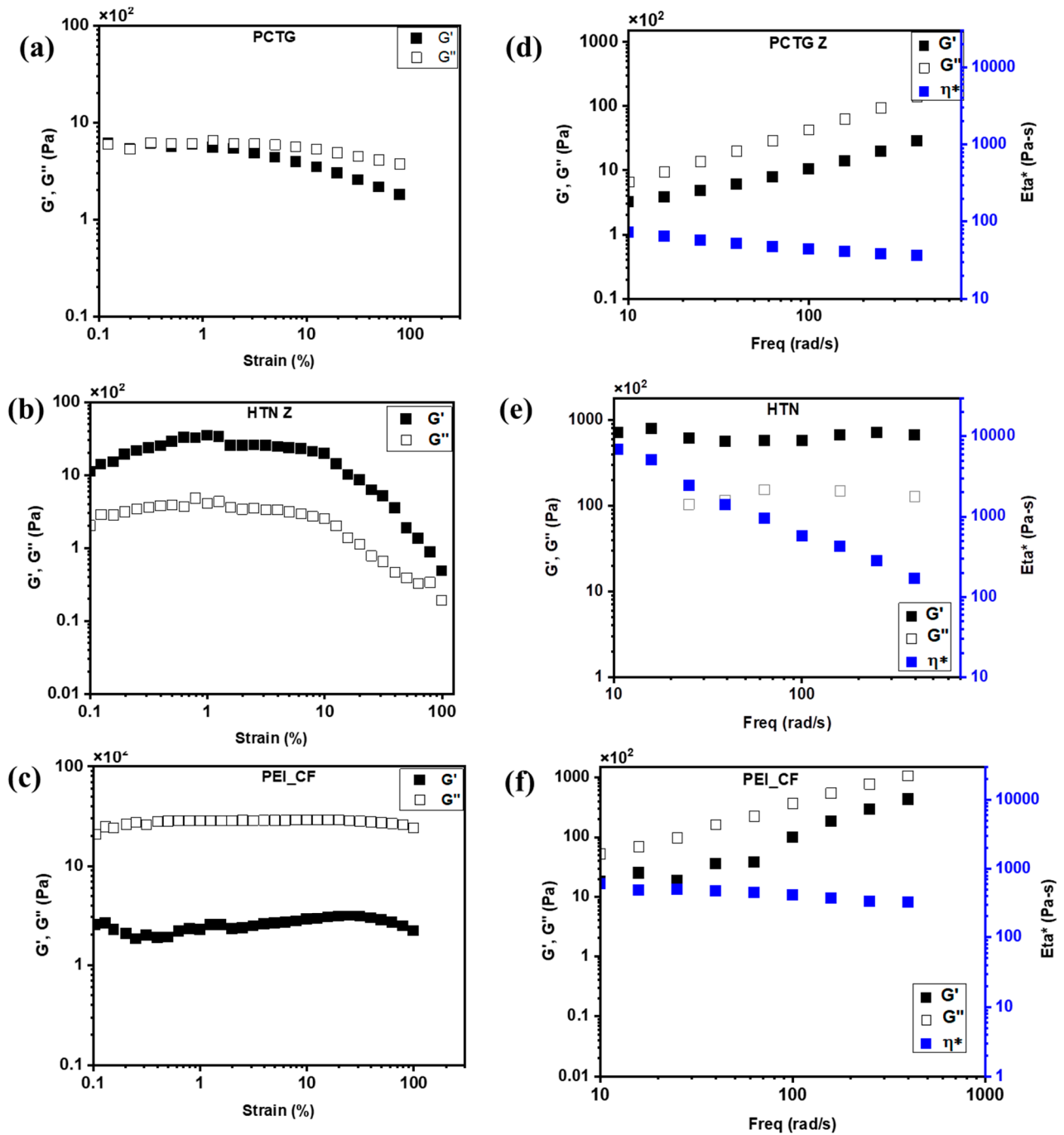


Figure 2. Strain sweep for (a) PCTG Z, (b) HTN Z, and (c) PEI-CF; frequency sweep for (d) PCTG Z, (e) HTN Z, (f) PEI-CF.

A power law model was applied to the dynamic frequency sweep curve, and the results are tabulated in Table 2. The dynamic frequency sweep was carried out in the linear viscoelastic region for all polymers. All the polymer systems showed a power law index n lower than 1, with HTN Z showing the lowest value and a prominent shear thinning

behavior among the selected polymer systems. The shear thinning behavior was found to be lower for PCTG Z and PEI-CF, with the power index closer to 1.

Table 2. The volumetric flow rates (Q) for optimized parameters, power law indices (n), and coefficient of determination R^2 .

	Q (mm ³ /s)	n	R^2
PCTG Z	7.2	0.813	0.987
HTN Z	4.8	0.035	0.998
PEI-CF	7.2	0.843	0.88

For PCTG (Figure 2d), the G'' was higher than G' across all frequencies, and both increased with frequency. A shear thinning effect was observed for PCTG Z; it was notable that the complex viscosity was significantly lower compared with the other two polymer systems used in this study. In the case of HTN Z, both G' and G'' were independent across the frequency range tested. The elastic component was dominant over the viscous component. The complex viscosity showed a predominant shear thinning effect for HTN Z. For PEI-CF, the viscous component was more dominant than the elastic component across the frequency. With the increase in the frequency, both G' and G'' increased [28]. Shear thinning behavior was observed for PEI-CF; however, in the dynamic frequency sweep, the drop in viscosity was marginal.

Steady state parallel-plate flow sweep was carried out for the polymer systems and is shown in Figure 3. This is more representative of the flow in the nozzle. For PCTG Z, the steady-state viscosity and dynamic viscosity were similar, which suggests that PCTG Z follows the Cox–Merz rule (Equation (3)). The steady state flow sweep of PEI-CF shows a critical strain around 10 s^{-1} , beyond which a shear thinning behavior is observed. In the HTN Z composite, there is an initial shear thinning region observed until 10 s^{-1} , above which it plateaus and then starts to drop off around 300 s^{-1} . The viscosities observed for steady state flow were lower for HTN Z and PEI-CF compared with the dynamic frequency sweep. From the literature, it is reported that for filled systems, the reduction in steady-state viscosity can be attributed to the fiber alignment in the direction of shear [29]. This is the most likely encountered condition during the material extrusion process of printing at the nozzle.

$$\eta(\dot{\gamma}) = \eta^*(\omega) \text{ for } \dot{\gamma} = \omega \quad (3)$$

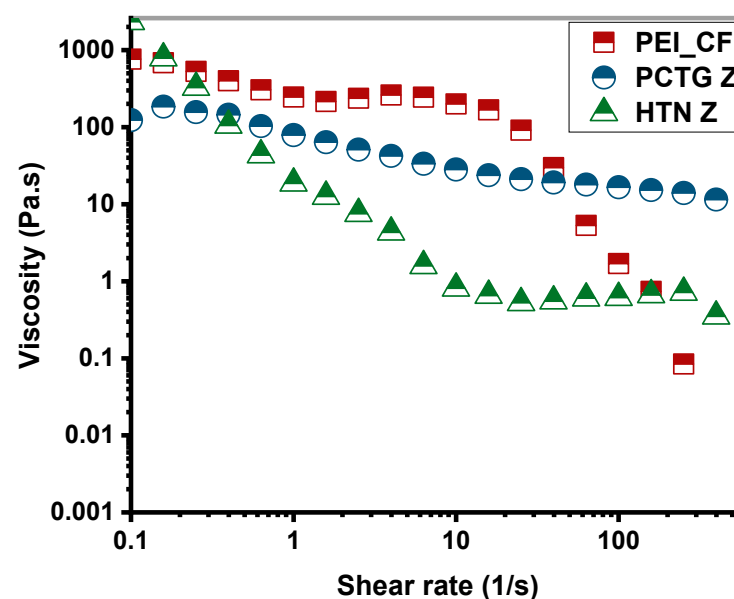


Figure 3. Steady flow shear sweeps for selected polymers.

From the steady state flow sweep, it was found that the steady-state viscosity of PCTG Z is higher than that of HTN Z and PEI-CF for the shear rates experienced around the nozzle region, contrary to the observations made in the dynamic frequency sweep.

Overall, from the rheological perspective, the following conclusions can be drawn: In both PCTG Z and PEI-CF, the viscous component dominated the elastic component across all frequencies. Although the polymer melt may be extruded from the nozzle at low viscosities, it may require longer relaxation times to retain and form a stable bead during the printing process [30,31].

In Z print, retention of shape and chain mobility play a critical role [32]. The polymer, which has a dominant elastic component and higher viscosity, ensures the stability of the printed parts. For PCTG Z, the viscous dominant nature and higher viscosity (from steady state flow) at shear rate experienced at the nozzle might pose significant challenges during printing. For HTN Z, it can be assumed that the filament can produce parts with the desired part geometry and performance due to its high viscosity and dominant elastic property.

3.2. FDM-Printed Parts of PCTG Z and HTN Z Using Single, Two-, and Four-Tensile-Bar Designs

Figure 4a shows that the single tensile bar failed to print with PCTG Z in the ZX build orientation due to an increased heat buildup issue and its rheological properties. Since the deposition time is short, it does not allow the cooling of the previously laid bead. This results in sagging of the material and instability of the part [19]. However, HTN Z showed a dominant elastic component, hence, a stable bead can be printed using HTN Z. This clearly indicates that the material flow properties are an important consideration for setting the print parameters for vertically built components. For comparison between the selected polymer systems, a single tensile bar design was not considered in this study.

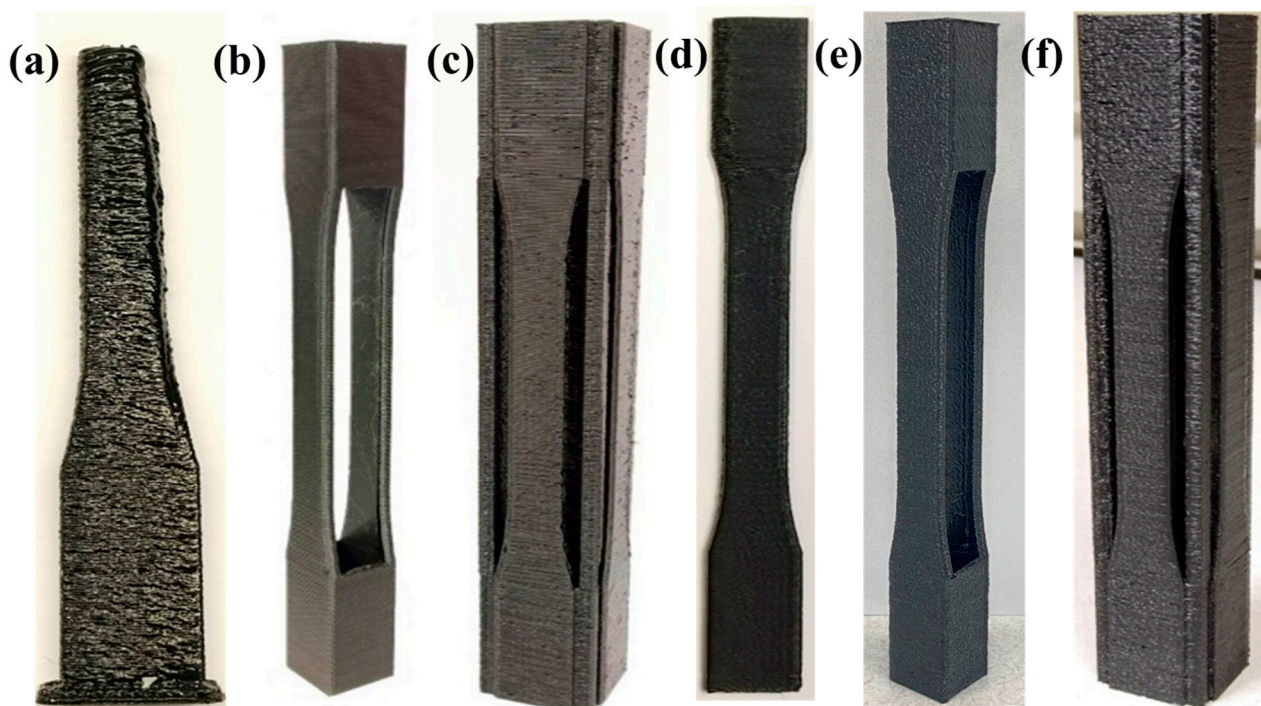


Figure 4. (a) PCTG Z single tensile bar; (b) PCTG Z 2B and (c) PCTG Z 4B; (d) HTN Z single tensile bar; (e) HTN Z 2B print; (f) HTN Z 4B samples.

The printed 2B and 4B PCTG Z (Figure 4b,c) and HTN Z (Figure 4d,e) are shown in Figure 4. The calculated layer time for 2B in the testing region was 7 to 8 s and for the 4B design was 23 s in the testing region.

3.3. Design Modification for PEI-CF

The two- and four-tensile-bar designs used for printing the PCTG Z and HTN Z did not work for printing the PEI-CF in the ZX direction. While printing PEI-CF using the two-tensile-bar design in the ZX build orientation, the part printed properly until the transition section but produced a consistent defect at the transition point from the testing section to the gripping section, as shown in Figure 5a. This point acted as a crack initiation point upon loading during the tensile testing, leading to premature failure of the coupons. The steady state shear sweep showed the high shear thinning nature of the PEI-CF material, which causes bead drooling and blobs, as seen in Figure 5a. The tested specimens of PEI-CF printed using two-tensile-bar designs are shown in Figure 4b. The fracture parts indicate premature failure of parts in these defect regions.

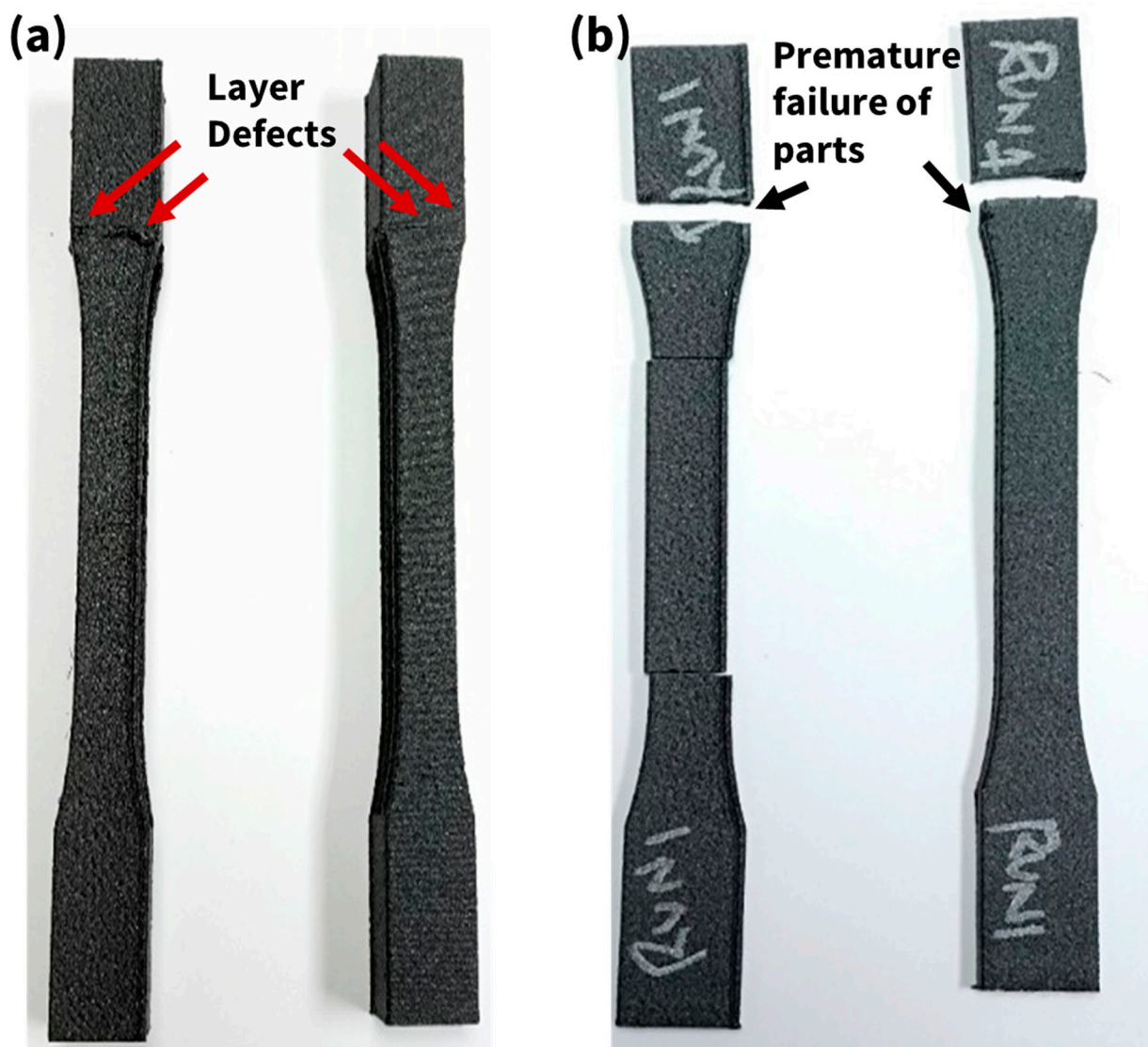


Figure 5. (a) The 2B print PEI-CF sample; (b) photos showing premature failure of tensile tested samples.

A different design was adopted to print the CF-PEI in the ZX build orientation to overcome these defects. The outline connections joining the edges in the top gripping section that connects the two tensile bars were removed, as shown in Figure 6a. Similarly, the 4B design was also modified (Figure 6a). The same design could be used for another polymer system, too.

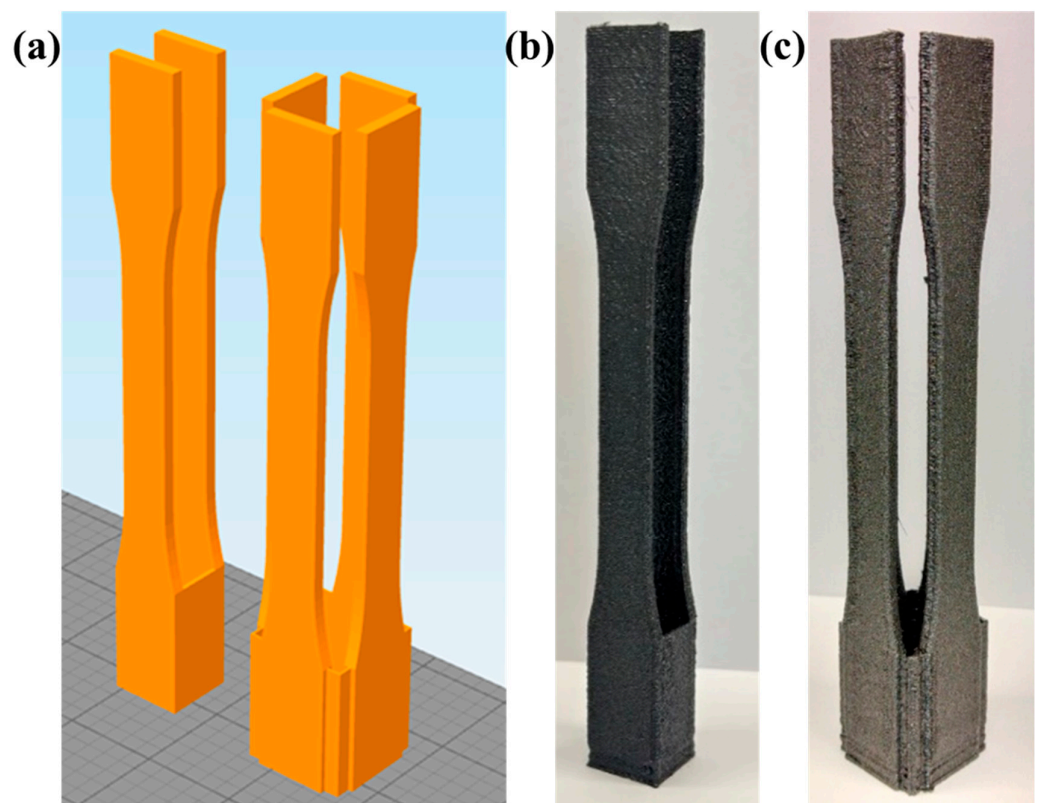


Figure 6. (a) Modified 2B and 4B design and (b,c) the successfully printed PEI-CF tensile bars.

The distance between the tensile bars was kept constant at 12 mm as in the two-tensile-bar design. The single outline connecting the 4B design was removed, as shown in Figure 6a, with the distance between the consecutive tensile bars remaining the same. The modified design (Figure 6a) was used to print the DoX to optimize the print parameters, and the calculated layer time for the modified design was 13–14 s.

3.4. DoX Study and Mechanical Properties

For the DoX study, two factors were considered: extrusion temperature and layer height. Table 3 shows the run order generated from Minitab, and Figure 7 shows the tensile strength obtained for various run orders. For PCTG Z, the higher layer height provided slightly higher strength at all print temperatures. A lower temperature of 290 °C, and layer height of 0.3 mm, was found to be the optimum print parameter. Studies have shown that lower height improves the interlayer adhesion; however, the print job time is inversely proportional to the layer height [33]. PCTG Z is predominantly viscous in nature, as reported in the previous section. An increased dwell time during the print job might cause print defects and sagging of the beads due to the heat buildup in the vertically built ZX samples and the viscous nature of the polymer.

Table 3. DoX designs for PCTG Z, HTN Z, and PEI-CF.

Run Order	PCTG Z		HTN Z		PEI-CF	
	Extrusion Temperature (°C)	Layer Height (mm)	Extrusion Temperature (°C)	Layer Height (mm)	Extrusion Temperature (°C)	Layer Height (mm)
1	290	0.2	340	0.2	430	0.2
2	310	0.2	320	0.2	450	0.3
3	290	0.3	320	0.3	430	0.3
4	310	0.3	340	0.3	450	0.2

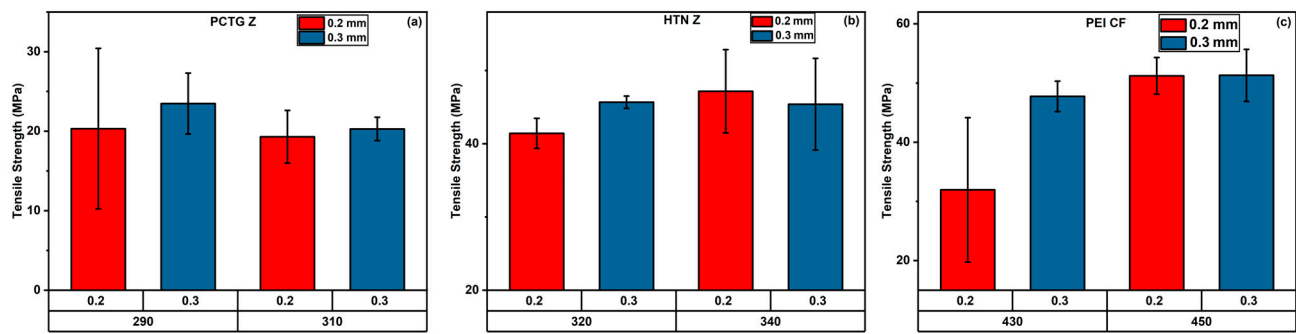


Figure 7. Tensile strength properties obtained for DoX runs for (a) PCTG Z, (b) HTN Z, and (c) PEI-CF a.

For HTN Z, the influence of the layer height and extrusion temperature factors was negligible. The semi-crystalline nature and predominantly elastic dominant nature of HTN Z should help in processing a stable bead onto the bed. A higher temperature and lower height will promote interlayer adhesion and diffusion. Accordingly, a higher extrusion temperature of 340 °C and 0.2 mm layer height gave the best tensile properties.

For PEI-CF, the temperature effect was more significant, with the highest strength properties achieved at 450 °C. The high temperature might improve the interlayer adhesion and diffusion of the PEI-CF system. The mobility of the polymer is hindered in this system due to the presence of carbon fiber filler, and hence, a higher extrusion temperature was found favorable in improving the diffusion and strength properties.

Table 4 indicates the optimized parameters, extrusion temperatures, and layer height for the three composites, and the other main processing parameters used for printing the two-tensile-bar designs. The same print process parameters were used to print the four-tensile-bar design print PEI-CF, and the retraction settings for PCTG Z and HTN Z were varied. Table 5 indicates the retraction settings for printing the four-tensile-bar designs while keeping the other print process parameters the same.

Table 4. Optimized process parameters from DoX.

Parameter	Composite		
	PEI-CF	PCTG Z	HTN Z
Extrusion temperature (°C)	450	290	340
Layer height (mm)	0.3	0.3	0.2
Print speed (mm/s)	40	40	40
Build plate temperature (°C)	160	80	80
Chamber temperature (°C)	90	50	80
Nozzle diameter (mm)	0.6	0.6	0.6
Extrusion width (mm)	0.6	0.6	0.6
Extrusion multiplier	1	1	1
Retraction distance (mm)	4.5	6	3
Extra restart distance (mm)	0	0	0
Retraction vertical lift (mm)	1	1	0.5
Retraction speed (mm/s)	30	30	30
Top solid layers	2	2	2
Bottom solid layers	2	2	2
Outlines	1	1	1
Infill angle	±45	±45	±45
Outline overlap (%)	40	40	40
Fan speed (%)	Not used	25	25

Table 5. Print process parameters for four-tensile-bar design.

Parameter	Composite	
	PCTG Z	HTN Z
Retraction distance (mm)	5	7
Extra restart distance (mm)	0	0
Retraction vertical lift (mm)	0.5	0.5
Retraction speed (mm/s)	30	30

3.5. Comparison of the Different Designs' Mechanical Properties

Figure 8a shows the results of tensile strength and Young's modulus comparison for the 2B and 4B designs of PCTG Z, HTN Z, and CF-PEI.

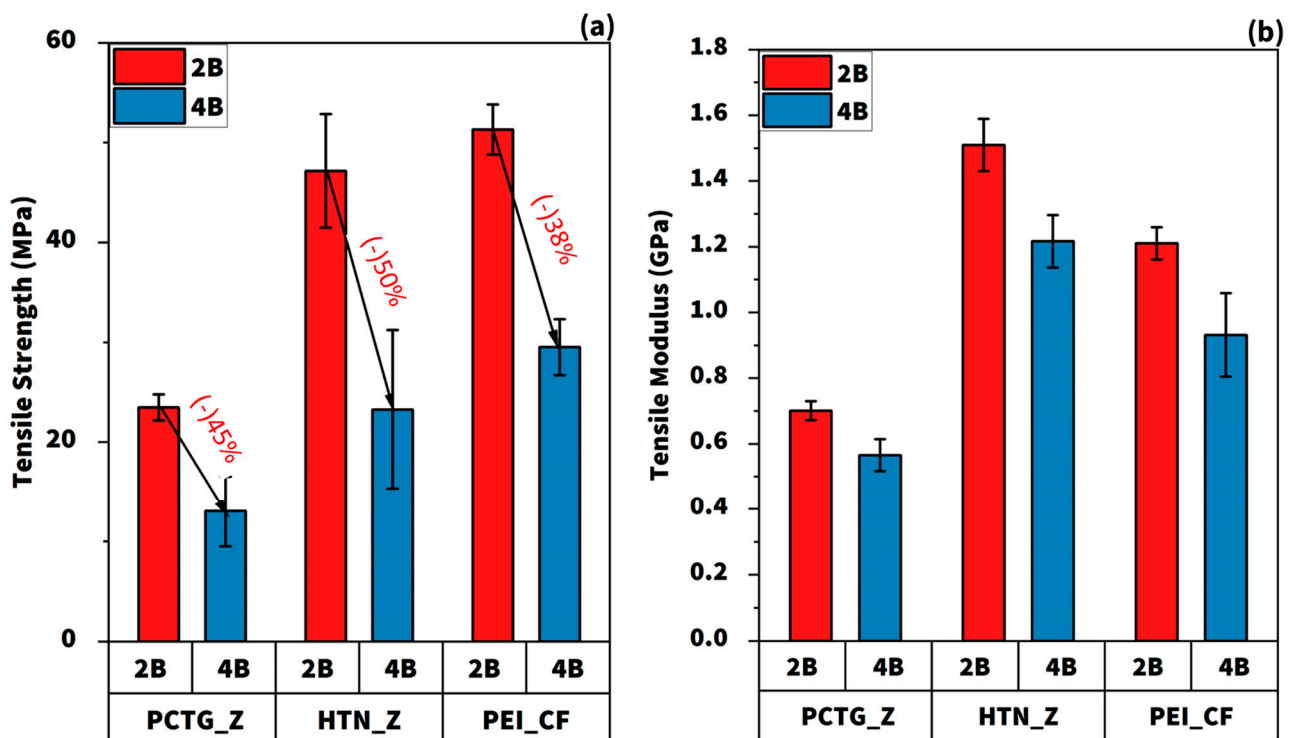


Figure 8. (a) The tensile strength for the two designs under consideration and (b) the tensile modulus for the two designs under consideration.

From Figure 8a, the tensile strength for the 2B design is higher than the 4B design for all the composites considered. The highest tensile strength among all the samples printed in the ZX build orientation is obtained with the PEI-CF, with a strength of 51.3 MPa due to the inherent material property. HTN Z also recorded a tensile strength of 47.2 MPa. The tensile strength obtained for PEI-CF and HTN Z declined by 38% and 50%, respectively, upon changing the design for printing the tensile bars from a 2B design to a 4B design. For PCTG Z, a tensile strength of 23.4 MPa and 13.0 MPa was obtained for two- and four-tensile-bar designs, respectively. In Section 3.1, it was suggested that printing PCTG Z and PEI-CF with a longer relaxation time after material deposition will produce a stable bead due to its dominant viscous nature. However, the tensile strength of 4B, which has a higher layer time, showed lower strength in all cases. This might be due to the deposited part cooling down below its T_g for amorphous polymers or crystallization of the part, in the case of PCTG Z, due to longer layer time. Interestingly, during the steady state shear flow test, it was found that PCTG Z has a higher viscosity at the shear rates experienced near the nozzle, and the power law index was higher for PCTG. This suggests that PCTG Z shows a lower dependence on shear rate, and hence, printing PCTG Z is more challenging. In the

case of HTN, which has a characteristically faster crystallization rate, it showed the highest drop in Z strength when the design was changed from 2B to 4B. This suggests that the layer time in the case of 4B is higher to start the crystallization of HTN Z, which, in turn, affects the interlayer bonding and diffusion process. The drop in the case of PEI-CF was lower compared with the other two cases due to the design modification, which resulted in reduced layer time.

Figure 8b indicates that the parts printed using PEI-CF and PCTG Z are stiffer when printed using a 2B design. A drop of 22% upon usage of 4B was observed for both materials. The HTN Z tensile modulus data demonstrated a more consistent stiffness for the parts printed with both designs, with the 2B design obtaining the higher tensile modulus of 1341.7 (± 72.5) MPa, and it dropped by only 10% for the 4B design.

From the mechanical test of the 2B and 4B, the 2B design was found to be the optimum design to achieve a good tensile property. Davies et al. suggested that the interlayer bonding strength is directly related to the diffusion process [9]. During the layer-to-layer deposition, the amorphous phase diffuses across the layers, which in turn is related to the local temperature at the interlayer surface. Layer time plays an important role in determining the local surface temperature. Ideally, a single tensile bar will have the lowest layer time and hence would give better strength properties. However, in most polymer systems, due to the heat buildup with layer-to-layer deposition, it is difficult to print without defects in the part. In this study, since the layer time was lower for the 2B design, better interlayer diffusion was observed. Hence, while printing a ZX bar, it is important to consider a design that has an optimum layer time.

To understand the failure mechanism and print quality for the two designs, SEM of the failed tensile coupons was carried out. The fracture surface morphology of PCTG Z is shown in Figure 9a,b for the 2B and 4B design. In the 2B sample, river marks and shear bands originating from the $\pm 45^\circ$ infill were observed. For PCTG Z, in the 2B design, inter-bead voids and small physical gaps were observed between the infill and the outline [34]. When the design was changed to 4B, a large physical gap between the outline and the infill was observed. However, no intra-bead voids were observed. Also, within the infill, the diffusion of the polymer is poor, and the boundary between them is visible. Since PCTG Z is a slow-crystallizing polymer, it can be assumed that the layer time is too short to initiate the crystallization. Hence, amorphous molecular diffusion might play a significant role in the interlayer bonding. The inter-bead voids suggest that at a longer layer time for the 4B design, the part cools below its glass transition temperature, which inhibits the molecular diffusion supported by the relatively higher viscosity reported from the steady flow strain sweep.

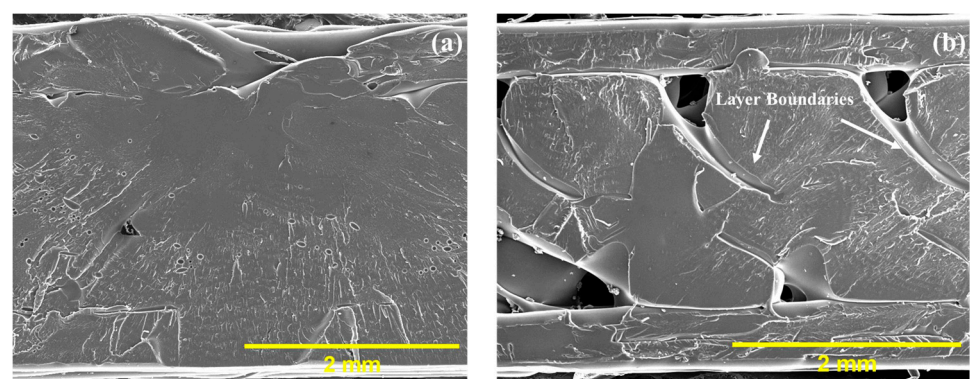


Figure 9. Tensile fracture morphology of PCTG Z (a) 2B and (b) 4B designs.

For HTN Z (Figure 10a), the fracture surface of the 2B design shows micro-texture flow, shear bands, and regions of fusion boundary. The presence of fusion boundary and secondary plateaus (Figure 10a) suggests a good interlayer bonding in the 2B design. This suggests amorphous molecular diffusion was better in the 2B design; however, when the

design was changed to 4B, the increased layer causes suboptimal interlayer diffusion. For the 4B design, the fracture surface was smooth (Figure 10b), with river marks and shear bands [35]. The river lines spread along the direction of crack propagation from the crack tip, leading to premature failure.

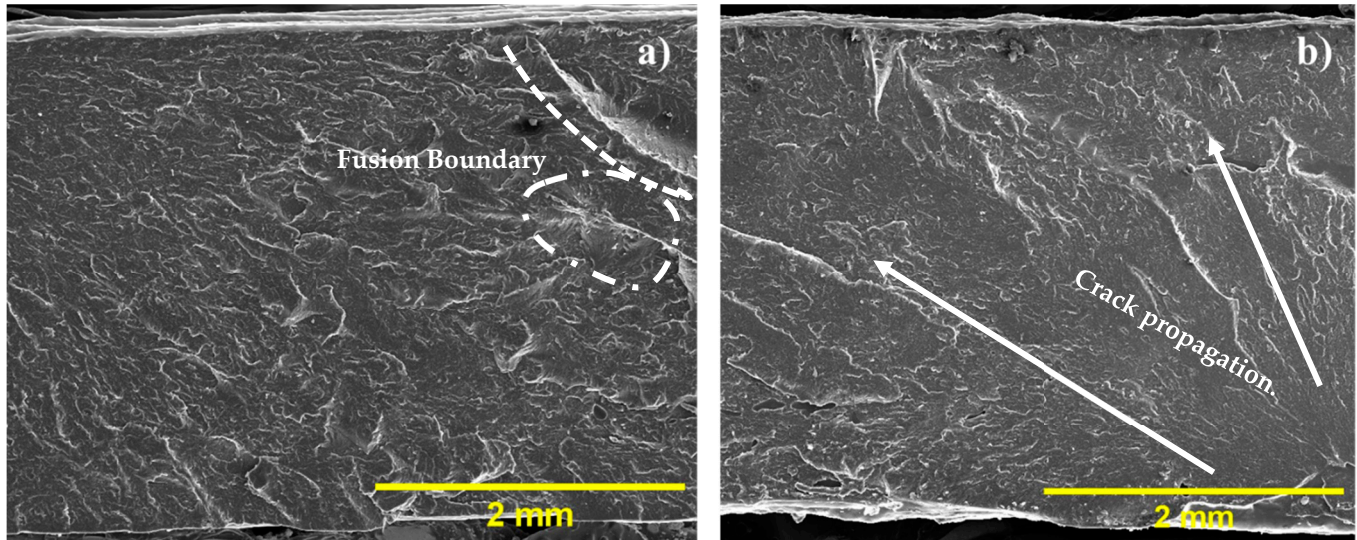


Figure 10. Tensile fracture morphology of HTN Z (a) 2B and (b) 4B designs.

In the case of PEI-CF (Figure 11a,b), large porosity and voids were observed. The high porosity was observed due to the presence of the reinforcement and the flow and coefficient of thermal expansion mismatch between carbon fiber fillers and polymer during the melt-extrusion/cool-down process. Compared with the 2B design, the 4B design shows smooth regions, which reveals that at higher layer times, the part cools below the T_g , and hence, a suboptimal cohesion and interlayer diffusion was observed. This could be a possible reason for the lower strength observed for the 4B design.

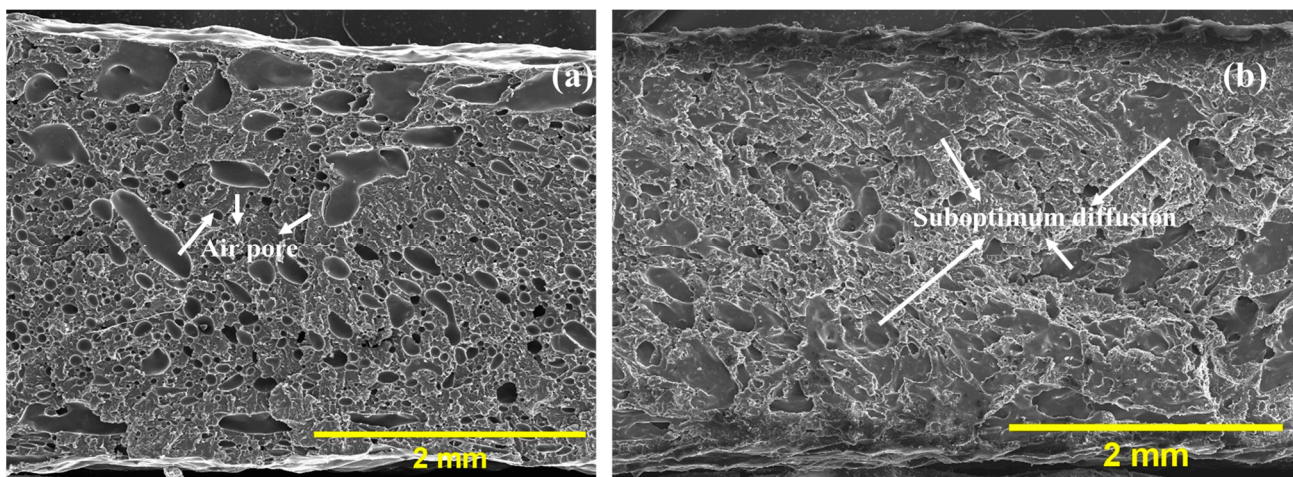


Figure 11. Tensile fracture morphology of PEI-CF (a) 2B and (b) 4B designs.

4. Conclusions

The study examined three different polymer systems, each with distinct physical and chemical properties, printed in the ZX orientation using two different designs. The findings highlight the crucial role of both the flow characteristics and the inherent nature of the polymer in ZX printing. Specifically, when the viscous component of a polymer is dominant, the relaxation time becomes vital in laying down a stable bead. It was observed

that a single tensile bar could not be successfully printed for PCTG Z and PEI-CF, whereas HTN Z allowed for the successful printing of a single bar. Rheological data provided key insights into the flow properties of the polymer systems, which could be used effectively to select appropriate print parameters. Among the various factors, layer time emerged as the most influential in determining the final mechanical properties, particularly the strength properties. The 2B design, which featured a shorter layer time, demonstrated better strength properties compared with the alternatives. SEM micrographs of the fractured surfaces revealed that longer layer times led to suboptimal cohesion and interlayer diffusion. The design of experiment (DoX) underscored the importance of considering multiple factors that influence mechanical properties, with the data from DoX being instrumental in optimizing the print parameters for both the 2B and 4B designs. Additionally, the retraction settings were found to be critical for successful ZX printing, especially in the production of complex structures. The lack of standardization in Z tensile methodology within the additive manufacturing (AM) community poses a challenge to the reliability and broader adoption of the technology. Therefore, there is a pressing need for the AM community to develop standardized testing methods for the ZX orientation. This work demonstrated that the 2B design could be confidently used across various material systems if the process parameters are optimized. Furthermore, the study emphasizes the importance of reporting both the layer time and design used in printing ZX orientation test coupons, as the proposed design not only enhances data reliability but also reduces post-processing requirements and material wastage.

Author Contributions: Conceptualization, A.K.K. and J.G.L.; methodology, R.R., A.K.K. and J.G.L.; validation, R.R., A.K.K. and J.G.L.; formal analysis, R.R. and A.K.K.; investigation, R.R. and A.K.K.; resources.; data curation, R.R. and A.K.K.; writing—original draft preparation, R.R. and A.K.K.; writing—review and editing, A.K.K. and J.G.L.; visualization, A.K.K. and J.G.L.; supervision, A.K.K. and J.G.L.; project administration, J.G.L.; funding acquisition, J.G.L. All authors have read and agreed to the published version of the manuscript.

Funding: The authors acknowledge the partial financial support provided by the Polymer Institute and the College of Engineering.

Data Availability Statement: The original contributions presented in the study are included in the article, further inquiries can be directed to the corresponding author/s.

Acknowledgments: The authors thank the Center for Materials and Sensor Characterization (CMSC) for assisting with the characterization work.

Conflicts of Interest: The authors declare no conflict of interest.

References

1. Xu, N.; Ye, X.; Wei, D.; Zhong, J.; Chen, Y.; Xu, G.; He, D. 3D artificial bones for bone repair prepared by computed tomography-guided fused deposition modeling for bone repair. *ACS Appl. Mater. Interfaces* **2014**, *6*, 14952–14963. [\[CrossRef\]](#)
2. Long, J.; Gholizadeh, H.; Lu, J.; Bunt, C.; Seyfoddin, A. Application of fused deposition modelling (FDM) method of 3D printing in drug delivery. *Curr. Pharm. Des.* **2017**, *23*, 433–439. [\[CrossRef\]](#)
3. Sonaye, S.Y.; Bokam, V.K.; Saini, A.; Nayak, V.V.; Witek, L.; Coelho, P.G.; Bhaduri, S.B.; Bottino, M.C.; Sikder, P. Patient-specific 3D printed Poly-ether-ether-ketone (PEEK) dental implant system. *J. Mech. Behav. Biomed. Mater.* **2022**, *136*, 105510. [\[CrossRef\]](#)
4. Alqurashi, H.; Khurshid, Z.; Syed, A.U.Y.; Habib, S.R.; Rokaya, D.; Zafar, M.S. Polyetherketoneketone (PEKK): An emerging biomaterial for oral implants and dental prostheses. *J. Adv. Res.* **2021**, *28*, 87–95. [\[CrossRef\]](#)
5. Kain, S.; Ecker, J.; Haider, A.; Musso, M.; Petutschnigg, A. Effects of the infill pattern on mechanical properties of fused layer modeling (FLM) 3D printed wood/polylactic acid (PLA) composites. *Eur. J. Wood Wood Prod.* **2020**, *78*, 65–74. [\[CrossRef\]](#)
6. Singh, J.; Goyal, K.K.; Kumar, R. Effect of filling percentage and raster style on tensile behavior of FDM produced PLA parts at different build orientation. *Mater. Today Proc.* **2022**, *63*, 433–439. [\[CrossRef\]](#)
7. Mohamed, O.A.; Masood, S.H.; Bhowmik, J.L. Process parameter optimization of viscoelastic properties of FDM manufactured parts using response surface methodology. *Mater. Today Proc.* **2017**, *4*, 8250–8259. [\[CrossRef\]](#)
8. Vaes, D.; Van Puyvelde, P. Semi-crystalline feedstock for filament-based 3D printing of polymers. *Prog. Polym. Sci.* **2021**, *118*, 101411. [\[CrossRef\]](#)

9. Kishore, V.; Chen, X.; Ajinjeru, C.; Hassen, A.A.; Lindahl, J.; Failla, J.; Kunc, V.; Duty, C. Additive manufacturing of high performance semicrystalline thermoplastics and their composites. In Proceedings of the Solid Freeform Fabrication 2016: Proceedings of the 26th Annual International Solid Freeform Fabrication Symposium—An Additive Manufacturing Conference, Austin, TX, USA, 8–10 August 2016; pp. 906–915.
10. Gao, X.; Qi, S.; Kuang, X.; Su, Y.; Li, J.; Wang, D. Fused filament fabrication of polymer materials: A review of interlayer bond. *Addit. Manuf.* **2021**, *37*, 101658. [\[CrossRef\]](#)
11. Ding, S.; Zou, B.; Wang, P.; Ding, H. Effects of nozzle temperature and building orientation on mechanical properties and microstructure of PEEK and PEI printed by 3D-FDM. *Polym. Test.* **2019**, *78*, 105948. [\[CrossRef\]](#)
12. Turner, B.N.; Gold, S.A. A review of melt extrusion additive manufacturing processes: II. Materials, dimensional accuracy, and surface roughness. *Rapid Prototyp. J.* **2015**, *21*, 250–261. [\[CrossRef\]](#)
13. Yu, W.; Wang, X.; Yin, X.; Ferraris, E.; Zhang, J. The effects of thermal annealing on the performance of material extrusion 3D printed polymer parts. *Mater. Des.* **2023**, *226*, 111687. [\[CrossRef\]](#)
14. Zaldivar, R.; Witkin, D.; McLouth, T.; Patel, D.; Schmitt, K.; Nokes, J. Influence of processing and orientation print effects on the mechanical and thermal behavior of 3D-Printed ULTEM® 9085 Material. *Addit. Manuf.* **2017**, *13*, 71–80. [\[CrossRef\]](#)
15. Zhang, H.; Wu, J.; Jia, M.; Chen, Y.; Wang, H. Enhancement on the mechanical properties of 3D printing PEI composites via high thermal processing and fiber reinforcing. *Polym. Adv. Technol.* **2023**, *34*, 3115–3124. [\[CrossRef\]](#)
16. Schöppner, V.; KTP, K.P. Mechanical properties of fused deposition modeling parts manufactured with Ultem® 9085. In Proceedings of the 69th Annual Technical Conference of the Society of Plastics Engineers (ANTEC'11), Boston, MA, USA, 1–5 May 2011; pp. 1–5.
17. Zaldivar, R.; McLouth, T.; Ferrelli, G.; Patel, D.; Hopkins, A.; Witkin, D. Effect of initial filament moisture content on the microstructure and mechanical performance of ULTEM® 9085 3D printed parts. *Addit. Manuf.* **2018**, *24*, 457–466. [\[CrossRef\]](#)
18. Chen, Q.; Zhang, Y.-Y.; Huang, P.; Li, Y.-Q.; Fu, S.-Y. Improved bond strength, reduced porosity and enhanced mechanical properties of 3D-printed polyetherimide composites by carbon nanotubes. *Compos. Commun.* **2022**, *30*, 101083. [\[CrossRef\]](#)
19. Davies, R.; Yi, N.; McCutcheon, P.; Ghita, O. Mechanical property variance amongst vertical fused filament fabricated specimens via four different printing methods. *Polym. Int.* **2021**, *70*, 1073–1079. [\[CrossRef\]](#)
20. Zarean, P.; Malgaroli, P.; Zarean, P.; Seiler, D.; de Wild, M.; Thieringer, F.M.; Sharma, N. Effect of printing parameters on mechanical performance of material-extrusion 3D-printed PEEK specimens at the Point-of-care. *Appl. Sci.* **2023**, *13*, 1230. [\[CrossRef\]](#)
21. Faes, M.; Ferraris, E.; Moens, D. Influence of inter-layer cooling time on the quasi-static properties of ABS components produced via fused deposition modelling. *Procedia Cirp* **2016**, *42*, 748–753. [\[CrossRef\]](#)
22. Li, Q.; Zhao, W.; Niu, B.; Wang, Y.; Wu, X.; Ji, J.; Li, Y.; Zhao, T.; Li, H.; Wang, G. 3D printing high interfacial bonding polyether ether ketone components via pyrolysis reactions. *Mater. Des.* **2021**, *198*, 109333. [\[CrossRef\]](#)
23. Pyl, L.; Kalteremidou, K.-A.; Van Hemelrijck, D. Exploration of specimen geometry and tab configuration for tensile testing exploiting the potential of 3D printing freeform shape continuous carbon fibre-reinforced nylon matrix composites. *Polym. Test.* **2018**, *71*, 318–328. [\[CrossRef\]](#)
24. Yıldız, A.; Emanetoğlu, U.; Yenigün, E.O.; Cebeci, H. Towards optimized carbon nanotubes (CNTs) reinforced polyetherimide (PEI) 3D printed structures: A comparative study on testing standards. *Compos. Struct.* **2022**, *296*, 115853. [\[CrossRef\]](#)
25. Miller, A.; Brown, C.; Warner, G. Guidance on the use of existing ASTM polymer testing standards for ABS parts fabricated using FFF. *Smart Sustain. Manuf. Syst.* **2019**, *3*, 122–138. [\[CrossRef\]](#)
26. Duty, C.; Ajinjeru, C.; Kishore, V.; Compton, B.; Hmeidat, N.; Chen, X.; Liu, P.; Hassen, A.A.; Lindahl, J.; Kunc, V. What makes a material printable? A viscoelastic model for extrusion-based 3D printing of polymers. *J. Manuf. Process.* **2018**, *35*, 526–537. [\[CrossRef\]](#)
27. Das, A.; Gilmer, E.L.; Biria, S.; Bortner, M.J. Importance of Polymer Rheology on Material Extrusion Additive Manufacturing: Correlating Process Physics to Print Properties. *ACS Appl. Polym. Mater.* **2021**, *3*, 1218–1249. [\[CrossRef\]](#)
28. Cossa, K.N. Basic concepts on rheology and application of shear-thickening fluids in protective gear. *SN Appl. Sci.* **2019**, *1*, 1–6. [\[CrossRef\]](#)
29. Ajinjeru, C.; Kishore, V.; Lindahl, J.; Sudbury, Z.; Hassen, A.A.; Post, B.; Love, L.; Kunc, V.; Duty, C. The influence of dynamic rheological properties on carbon fiber-reinforced polyetherimide for large-scale extrusion-based additive manufacturing. *Int. J. Adv. Manuf. Technol.* **2018**, *99*, 411–418. [\[CrossRef\]](#)
30. El Magri, A.; Vanaei, S.; Vaudreuil, S. An overview on the influence of process parameters through the characteristic of 3D-printed PEEK and PEI parts. *High Perform. Polym.* **2021**, *33*, 862–880. [\[CrossRef\]](#)
31. Salazar-Martin, A.G.; Garcia-Granada, A.A.; Reyes, G.; Gomez-Gras, G.; Puigoriol-Forcada, J.M. Time-Dependent Mechanical Properties in Polyetherimide 3D-Printed Parts Are Dictated by Isotropic Performance Being Accurately Predicted by the Generalized Time Hardening Model. *Polymers* **2020**, *12*, 678. [\[CrossRef\]](#)
32. Ajinjeru, C.; Kishore, V.; Chen, X.; Hershey, C.; Lindahl, J.; Kunc, V.; Hassen, A.A.; Duty, C. Rheological survey of carbon fiber-reinforced high-temperature thermoplastics for big area additive manufacturing tooling applications. *J. Thermoplast. Compos. Mater.* **2021**, *34*, 1443–1461. [\[CrossRef\]](#)

33. de Carvalho, W.S.; Marzemin, F.; Belei, C.; Petersmann, S.; Arbeiter, F.; Amancio-Filho, S.T. Statistical-based optimization of fused filament fabrication parameters for short-carbon-fiber-reinforced poly-ether-ether-ketone considering multiple loading conditions. *Polym. Test.* **2023**, *128*, 108207. [[CrossRef](#)]
34. Purslow, D. Some fundamental aspects of composites fractography. *Composites* **1981**, *12*, 241–247. [[CrossRef](#)]
35. Dhakal, N.; Wang, X.; Espejo, C.; Morina, A.; Emami, N. Impact of processing defects on microstructure, surface quality, and tribological performance in 3D printed polymers. *J. Mater. Res. Technol.* **2023**, *23*, 1252–1272. [[CrossRef](#)]

Disclaimer/Publisher’s Note: The statements, opinions and data contained in all publications are solely those of the individual author(s) and contributor(s) and not of MDPI and/or the editor(s). MDPI and/or the editor(s) disclaim responsibility for any injury to people or property resulting from any ideas, methods, instructions or products referred to in the content.